SMOS ESL 2019-2024

ESL for Geophysical (L3 & 4) data over land ice and sea ice

SMOS L3 Sea Ice Thickness ATBD

Initial Preparation by: Xiangshan Tian-Kunze   March 2nd 2021

Reviewed by: Lars Kaleschke   April 15th 2021

Reviewed by: Raffaele Crapolicchio   July 15th 2021

Revision by: Xiangshan Tian-Kunze   October 28th 2021

Alfred Wegener Institute, Helmholtz Centre for Polar and Marine Research
www.awi.de

Document Information

Contract Data	
Contract Number	ARG-003-081/SMOS-2020/AWI
Contract Issuer	ESA/ESRIN

Internal Distribution		
Name	**Organization**	**Copies**
José Barbosa	Deimos	1
Manuel Arias	Argans	1
Roger Balague	ZBT	1
Internal Confidentiality Level		
Unclassified ☑	Restricted	Confidential ☐

External Distribution		
Name	**Organization**	**Copies**
Raffaele Crapolicchio	ESA	1
Roberto Sabia	ESA	1

Archiving	
Word Processor	MS Word 2011
File Name	[DT4-1]-AWI-SMOS-T4-ATBD-v1.1.docx

Document Status and Change Log

version	Section	Change Description	Date
v0	All	Initial draft of L3 sea ice thickness ATBD and Validation Report v0	17/04/2020
v1	All	This version includes only the ATBD. A separate Validation Report v1 is submitted to ESA on 09/12/2020.	13/04/2021
v1.1	All	Revision according to the feedback from ESA (15 July, 2021).	28/10/2021

Table of Contents

List of Tables and Figures

1. Introduction

1.1. Motivation and purpose of the document

The purpose of this Algorithm Theoretical Basis Document is to describe the retrieval algorithm implemented to derive sea ice thickness from SMOS brightness temperatures at Alfred Wegener Institute, under the contract "**SMOS Expert Support Laboratory (ESL) for SMOS Level 1 and Level 2 over land, ocean and ice**". The current product consists of daily averaged sea ice thickness on the NSIDC grid in the polar-stereographic projection.

Thin sea ice plays a key role in the heat exchange between ocean and atmosphere in the polar regions. However, satellite-based observation of sea ice thickness is still very challenging. The first satellite borne observations of sea ice thickness were conducted with satellite radar altimeters carried on European Remote Sensing satellites (ERS-1 and ERS-2) (Laxon et al., 2003). These early radar altimeter observations were followed by the ICESat laser altimeter from 2003 to 2009 (Kwok et al., 2008) and since 2011 by the CryoSat-2 radar altimeter (Laxon et al., 2013). The radar and laser altimeters have large uncertainties for sea ice thickness less than 1 m (Laxon et al., 2003; Kwok et al., 2008). Therefore, they are more suitable for the detection of thick sea ice. Thin sea ice thickness up to around 0.5 m with 1 km spatial resolution can be estimated with thermal imagery based on ice surface temperature together with atmospheric forcing data through ice surface heat balance equation (Yu and Rothrock, 1996). The major drawback with this method is the requirement for cloud-free conditions, and thus, there may be long temporal gaps in the thickness chart coverage over a region of interest.

SMOS measures for the first time globally Earth's radiation at a frequency of 1.4 GHz in the L-band. The spatial resolution varies from about 35 km to more than 50 km. L-band radiometry on SMOS can be used to obtain the sea ice thickness, which is due to the large penetration depth in sea ice (Kaleschke et al., 2010; Kaleschke et al., 2012). The measured brightness temperature depends on the sea ice concentration, the molecular temperatures of the sea and the ice, and their emissivity. The sea ice emissivity depends on the sea ice microphysical structure but the inhomogeneities like brine pockets and air bubbles are much smaller than the wavelength of 21 cm. Therefore, we can consider sea ice as a homogeneous medium and neglect volume scattering. The modelled sea ice emissivity used for the present algorithm mainly depends on ice thickness, ice temperature, and ice salinity.

In contrast to ICESat and CryoSat-2 measurements, SMOS-derived sea ice thickness has less uncertainty in the thin ice range, but an exponentially increasing uncertainty for sea ice thickness thicker than 0.5 m. In our study we consider sea ice thickness less than 0.5 m as thin ice. SMOS-derived ice thickness can thus complement the measurements from CryoSat-2 to achieve Arctic-wide sea ice thickness estimations (Ricker et al., 2017).

This ATBD provides an elaborate description of the SMOS sea ice thickness retrieval algorithm with version number v3.2 and v3.3. Algorithm v3.2 is based on v620 L1C data, whereas Algorithm v3.3 is based on v724 L1C data. From 15 October , 2021 on the operational processing is switched to v724 SMOS L1C data.

Table 1. Product version reference

Version	Date	Comments
V3.2	15.10.2018	Official ESA release
V3.3	15. 10. 2021	Change of L1C version from v620 to v724; RFI filtering is updated based on RFI flags in the v724 L1C data; Polar stereographic projection is updated to EPSG:3413; Output file is given in NetCDF v4 instead of v3. More detailed information about v3.3 product can be found here: https://spaces.awi.de/display/CS2SMOS/SMOS+Sea+Ice+Thickness

1.2. Applicable documents

[SoW] SMOS Expert Support Laboratory (ESL) for SMOS Level 1 and Level 2 over land, ocean and ice, ESA-EOPG-MOM-SOW-70

[SM-TN-AURO-L1OP-0001] TN on the L1OP RFI Flags, 30/06/2020

[DT4-1a]   SMOS Ice Thickness ATBD v1.1, 28/10/2021, this document

[DT4-1b]   SMOS Ice Thickness PVR v2.1, 28/10/2021

[DT4-2]   CS2SMOS ATBD v2.0, 09/12/2020

1.3. Reference documents

[RD1]   SMOS Sea Ice Retrieval Study (SMOSIce) Final Report ESA ESTEC Contract No.: 4000101476/10/NL/CT

[RD2]   Tian-Kunze et al., "SMOS-derived thin sea ice thickness: algorithm baseline, product specifications and initial verification", The Cryosphere, 8, 997-1018, 2014 doi:10.5194/tc-8-997-2014

[RD3]   Kaleschke et al., "SMOS sea ice product: Operational application and validation in the Barents Sea marginal ice zone", Remote Sensing of Environment, 180 (2016) 264-273, doi:10.1016/j.rse.2016.03.009

For a full list of scientific references, see Section 6.

1.4. Acronyms and abbreviations

ATBD	Algorithm Theoretical Basis Documents
ESA	European Space Agency
ESL	Expert Support Laboratory
ESTEC	European Space Research and Technology Centre
L1	Level 1 product
L2	Level 2 product
MIRAS	Microwave Imaging Radiometer using Aperture Synthesis
MITgcm	MIT general circulation model
NSIDC	National Snow and Ice Data Center
PVR	Product Validation Report
RD	Reference Document
RFI	Radio Frequency Interference
rev.	revision
SMOS	Soil Moisture and Ocean Salinity
SoW	Statement of Work
SSS	Sea Surface Salinity
TN	Technical Note
v.	version

1.5. List of variables and constants

Table 2. List of variables

Variable name	Descriptive name	Units	ATBD reference	Comments
TB_h	Horizontally polarized brightness temperature	K	3.1, 4.1	From L1C data
TB_v	Vertically polarized brightness temperature	K	3.1, 4.1	From L1C data
TB	Brightness temperature intensity	K	3.1, 4.1	calculated
nPair	Number of pairs of TB_h and TB_v		3.1, 4.1	calculated
rfiratio	Percent of RFI-contaminated measurements in total measurements	%	3.2, 4.1	calculated
T_{ice}	Bulk ice temperature	K	4.4	calculated
S_{ice}	Bulk ice salinity	g/kg	4.4	calculated
d_{ice}	Plane layer ice thickness	m	4.4	calculated
d_{max}	Maximal retrievable ice thickness	m	4.4	calculated
S_w	Sea surface salinity	psu	4.4	Aux2
h_s	Snow thickness	m	4.5	calculated
k_i	Thermal conductivity of ice	W/m/K	4.5	calculated
F_r	Incoming shortwave radiation	W/m²	4.5	Reference table in Maykut, 1986
$(1-\alpha)F_r-I_0$	Net incoming shortwave radiation	W/m²	4.5	Reference table in Maykut, 1986
F_{Lin}	Incoming longwave radiation	W/m²	4.5	calculated
F_{Lout}	Outgoing longwave radiation	W/m²	4.5	calculated
F_s	Sensitive heat flux	W/m²	4.5	calculated
F_e	Latent heat flux	W/m²	4.5	calculated
F_c	Conductive heat flux	W/m²	4.5	calculated
T_{si}	Snow-ice interface temperature	K	4.5	calculated
T_s	Snow/bare ice surface temperature	K	4.5	calculated
u	10m wind speed	m/s	4.5	Aux1
T_a	2m surface air temperature	K	4.5	Aux1
ε^*	Effective longwave emissivity of atmosphere in the Arctic		4.5	calculated

e_{sa}	Saturation vapor pressure, air	hpa	4.5	calculated
e_{so}	Saturation vapor pressure, ice	hpa	4.5	calculated
H	Mean sea ice thickness, after correcting with sea ice thickness distribution function	m	4.6	calculated

Aux1: JRA55 reanalysis data

Aux2: Model output from MITgcm

Table 3. List of constants

Constant name	Descriptive name	Units	ATBD reference	Values	Reference
T_w	Sea water temperature	K	4.4, 4.5	271.25	Approximate value
S_R	Salinity ratio		4.4	0.175	Kovacs, 1996
a	Sea ice growth rate coefficient		4.4	0.5	Ryvlin, 1974
k_s	Thermal conductivity of snow	W/m/K	4.5	0.31	Yu and Rothrock, 1996
L	Latent heat of vaporization	kJ/kg	4.5	2257	Maykut, 1986
ρ	Density of air	kg/m^3	4.5	1.3	Maykut, 1986
c_p	Specific heat of the air	J/kg/K	4.5	1005	Maykut, 1986
Cs	the bulk transfer coefficient for sensible heat		4.5	$3.0*10^{-3}$	Maykut, 1986
Ce	the bulk transfer coefficient for latent heat		4.5	$3.0*10^{-3}$	Maykut, 1986
C	Cloud coverage		4.5	0.8	Approximate value
r	Relative humidity		4.5	0.4	Approximate value
P	Surface pressure	hpa	4.5	1000	Approximate value
ε_L	Longwave emissivity of ice		4.5	1	Maykut, 1986
σ	Stefan-Boltzman constant	W/m²/K^4	4.5	$5.67*10^{-8}$	

2. Algorithm overview

2.1. Retrieval structure

The present sea ice thickness is produced using an iterative retrieval algorithm (see section 4.7) that is based on a thermodynamic sea ice model and a three-layer radiative transfer model, which explicitly takes variations of ice temperature and ice salinity into account. In addition, ice thickness variations within the SMOS spatial resolution are considered through a statistical thickness distribution function derived from high-resolution ice thickness measurements from NASA's Operation IceBridge campaign.

The radiation model calculates the emissivity of the sea ice layer and the underlaying sea water. Brightness temperatures are derived from the emissivity and physical temperatures of sea ice and sea water. We use bulk ice temperature as the physical sea ice temperature since we apply only one ice layer. The bulk ice temperature is estimated from the thermodynamic model, using auxiliary 2m air temperature from atmospheric reanalysis data as input parameter. The following chart (Figure 1) shows the retrieval structure consisting the two models.
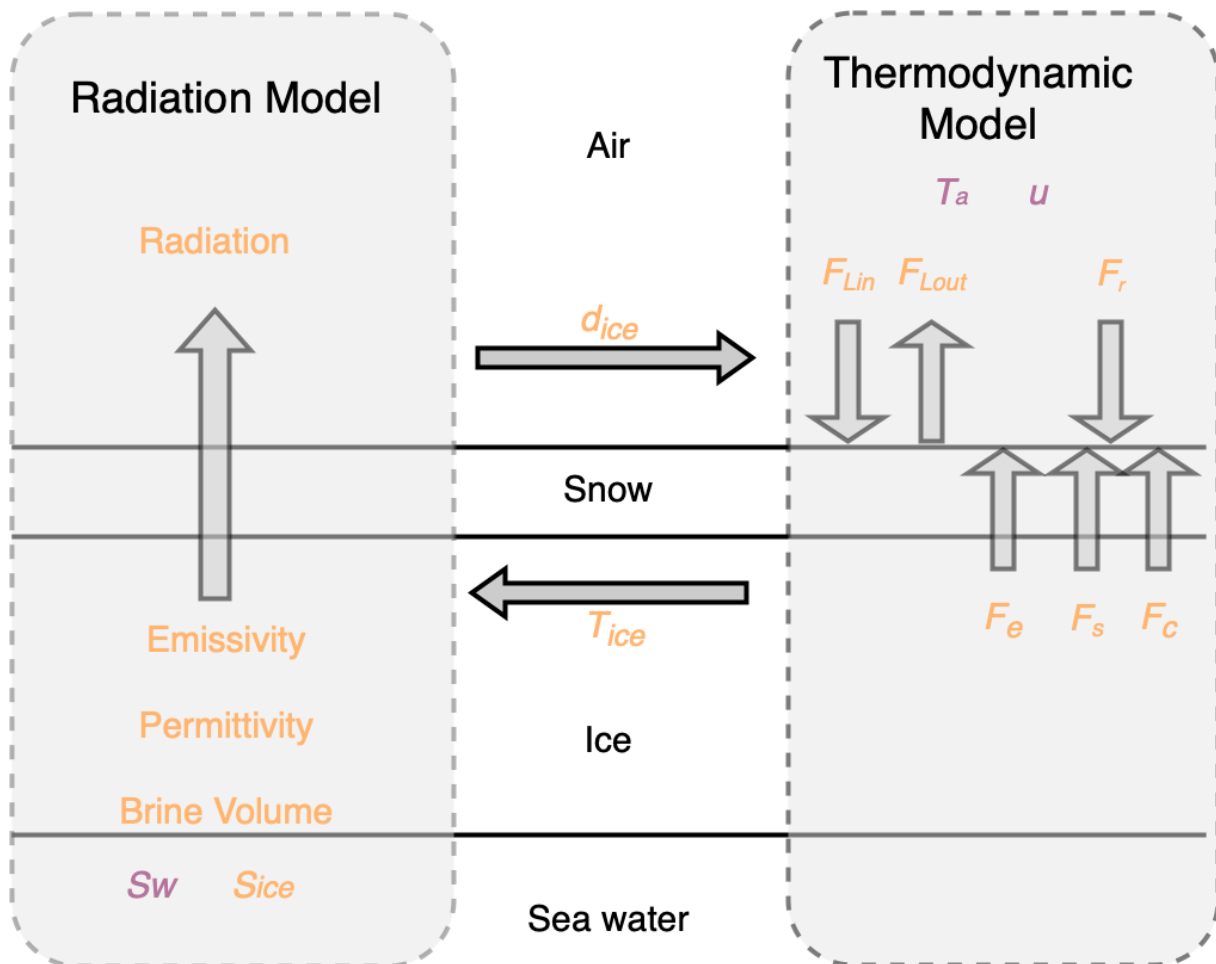

Figure 1. Retrieval structure with L-band brightness temperature radiation model and thermodynamic model. Variables in purple are input parameters from auxiliary data, in orange are calculated parameters in the retrieval model.

2.2. Sea Ice Thickness retrieval scheme

The sea ice thickness retrieval scheme is shown in figure 2. The processing is carried out in three steps: (1) An intermediate brightness temperature dataset L3A is generated from L1C data daily and saved in HDF file format on the local server. These files include all information provided in L1C swath data, but sorted by an equal-area grid system (15 Km, ISEA 4H9 grid, L1C data is provided on this grid system) grid points to ease the reading process of L1C swath files. (2) Gridded L3B brightness temperature data in NSIDC polar-stereographic projection with 12.5 km grid resolution are generated from L3A data for the northern and southern hemisphere each. (3) L3C ice thickness is generated from L3B brightness temperatures comparing to the pre-calculated look-up table, with JRA55 reanalysis and Sea Surface Salinity Climatology as auxiliary data. This L3C ice thickness data is disseminated via AWI ftp server (ftp.awi.de) and ESA data platform (https://smos-diss.eo.esa.int/oads/access/).
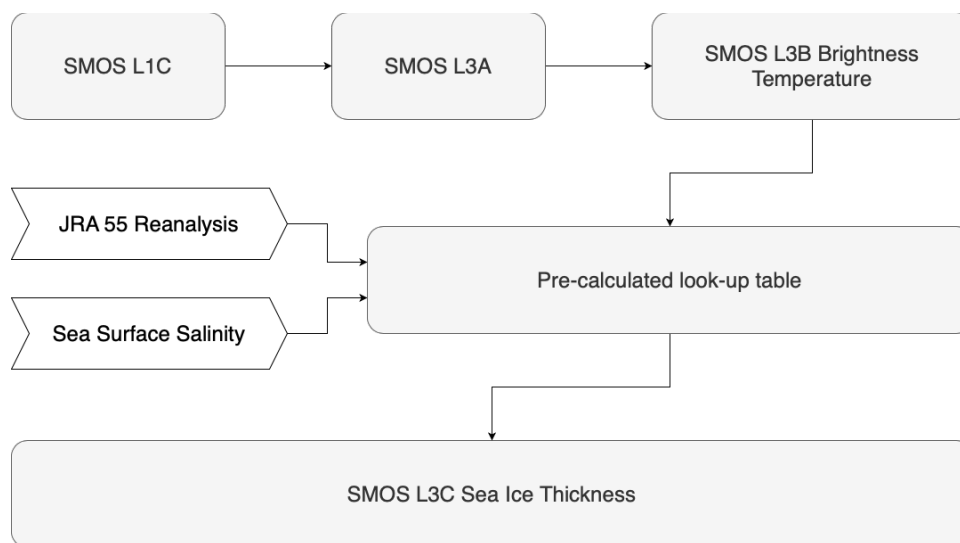
Figure 2. Schematic flow chart of SMOS sea ice thickness retrieval

3. Data availability and RFI

3.1. Data availability

SMOS has daily coverage in the Arctic up to 85° latitude for the incidence angle of 0-40° used in the present retrieval. Most of the grid points in the Arctic are covered by several SMOS swaths. In the Antarctic where sea ice occurs in much lower latitudes, areas with missing data exist, varying on daily basis. The parameter nPair, which is provided in the product, describes the number of TB_h and TB_v pairs used to calculate the daily average intensity and consists indirect information of the input data quality.

3.2. RFI filtering

SMOS measurements are partly influenced by Radio Frequency Interference (RFI) which comes from radars, TV and radio transmission (Mecklenburg et al., 2012). The RFI influence depends on the incidence angle, polarization, and ascending or descending orbit direction of the satellite

(Camps et al., 2010). A closer look into RFI-contaminated snapshots shows that RFI can either completely or partly destroy a snapshot (Camps et al., 2010). The status of RFI has improved much since 2010.

For our retrieval, we applied the RFI flag provided in v620 and v724 L1C data sets (SM-TN-AURO-L1OP-0001, 30/06/2020). Table 5 shows the usage of RFI flags in our retrieval algorithms v3.2 and v3.3. Additionally, we apply a threshold value for both horizontally and vertically polarized brightness temperatures. If either of them exceeds 300 K within one snapshot, this snapshot is considered RFI contaminated: all the measurements in the snapshot are rejected. Brightness temperatures higher than 300 K cannot be expected in the Arctic and Antarctic.

Table 4. RFI flags in L1C data that used in the sea ice retrieval

	Algorithm V3.2 based on v620 L1C data	Algorithm V3.3 based on v724 L1C data
Pixel-based RFI flag	RFI point source	RFI point source
	RFI tail source	RFI tail source
	NIR X/Y	
Snapshot field flag	Not exist	Exist but not used due to high data loss

The detection of RFI sources and the mitigation of RFI influence are critical steps for the further retrieval of geophysical parameters. Figure 3 shows the RFI-induced data loss based on our RFI filter. The RFI ratio in the figure is defined as the ratio between the number of RFI-contaminated measurements and the number of total measurements.
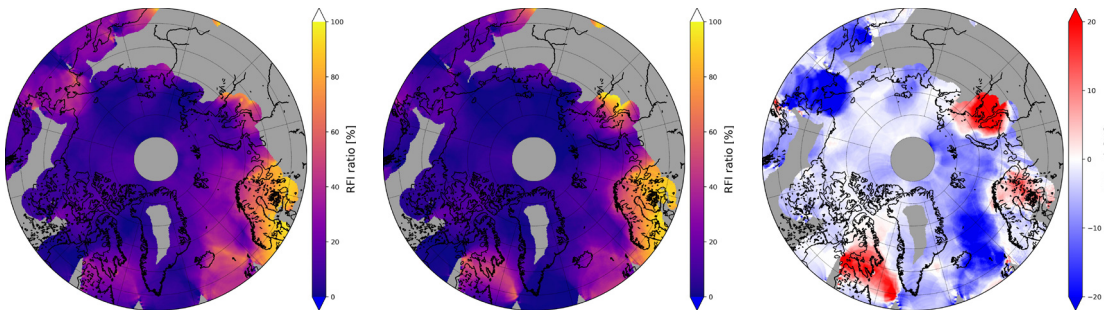
Figure 3. RFI ratio calculated from v620 (left) and v724 (middle) L1C data on October 15, 2017 based on the RFI flags and 300 K threshold value. The right figure shows the difference of the two version (v724-v620).

4. Algorithm description

4.1. Brightness temperature intensities

The SMOS payload Microwave Imaging Radiometer using Aperture Synthesis (MIRAS) measures in L-band the brightness temperatures in full polarization with incidence angles ranging from 0° to 65° (Kerr et al., 2001). All four Stokes parameters are obtained. It has a global coverage every three days, whereas daily coverage up to latitude 85° can be expected in the polar regions. Brightness

temperature is taken every 1.2 s by hexagon-like, two-dimensional snapshots which have a spatial dimension of about 1200 km across. The geometric distribution of incidence angles and radiometric accuracy within the alias-free areas of a snapshot is shown in Figure 4. The spatial resolution varies from about 35 km at nadir view to more than 50 km at incidence angles higher than 60°. Each snapshot measures one or two of the Stokes components in the antenna reference frame. Horizontally (TB_h) and vertically (TB_v) polarized brightness temperatures are measured by separate snapshots. The southern and northern boundaries of the polar regions are defined as latitude 50°N and 50°S for the sea ice thickness retrieval.

Over sea ice the first Stokes parameter (intensity) is almost independent of incidence angle in the incidence angle range of 0°-40° (Figure 5). The intensity is the average of the horizontally (TB_h) and the vertically polarized (TB_v) brightness temperatures. The intensity is independent of both geometric and Faraday rotations and robust to instrumental and geophysical errors (Camps et al., 2005). We can avoid additional uncertainties caused by the transformation from the antenna reference frame to the Earth reference frame by using the intensity. By using the whole incidence angle range of 0°-40° we can significantly reduce the uncertainty caused by individual brightness temperature measurement. However, at the same time by averaging all the daily measurements we smooth out partly the geophysical and temporal variability. The daily averaged brightness temperature intensities in the Arctic and in the Antarctic are interpolated with nearest neighbor algorithm and gridded into the National Snow and Ice Data Center (NSIDC) polar stereographic projection with a grid resolution of 12.5 km (see for detailed description in section 5)
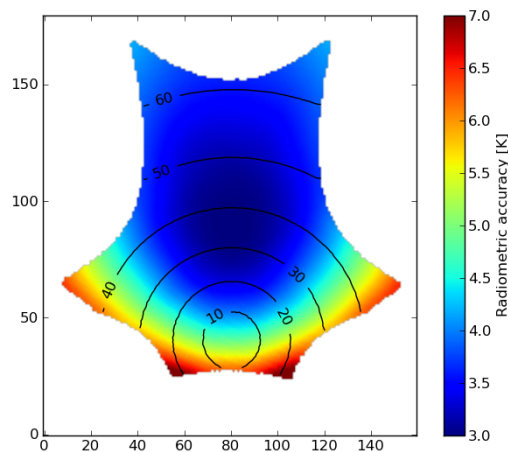

Figure 4. Geometric distribution of incidence angles with respective radiometric accuracy.
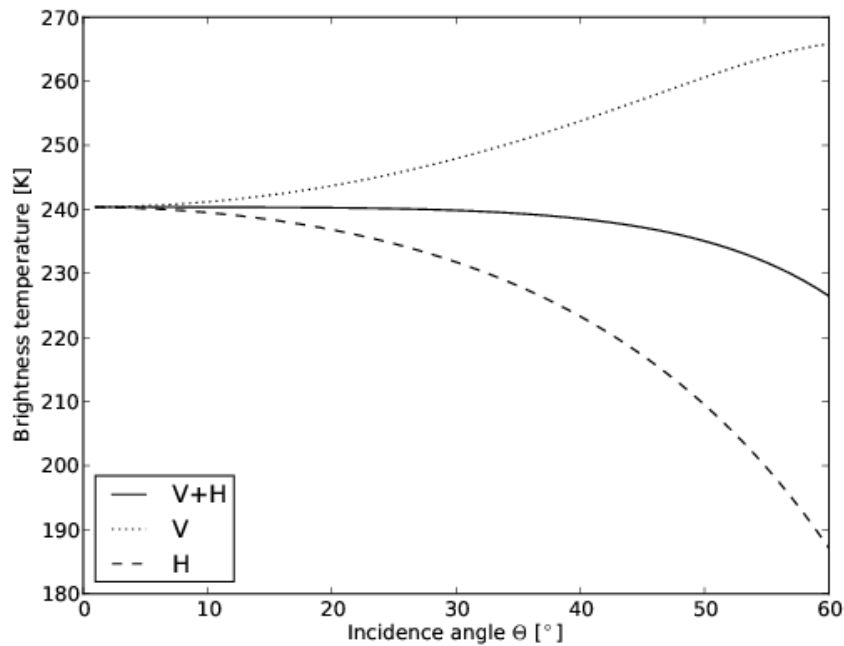
Figure 5. Simulated horizontally and vertically polarized brightness temperatures at different incidence angles using Fresnel equations. The intensity, which is the average of both remains almost constant in the incidence angle range of 0°-40°.

4.2. JRA55 reanalysis data

To estimate ice surface temperature, we extract the 2 m surface air temperature and the 10 m wind velocity data from JRA-55 atmospheric reanalysis data and interpolate them using GMT surface command (http://gmt.soest.hawaii.edu/doc/latest/surface.html) into the polar stereographic projection with 12.5 km grid resolution. JRA-55 reanalysis data provide various physical variables in 1.125° resolution every six hours. For SMOS retrieval we consider three previous days temperature and wind field data and average them to run the thermodynamic model. We assume in the thermodynamic model an immediate equilibrium at air-ice surface, therefore, an average of several days data is necessary to avoid the impact of abrupt temperature change on the sea ice thickness retrieval. The data has been produced by the Japanese Meteorological Agency using the latest numerical analysis and prediction system. The same reanalysis data is used for both the operational and reprocessed data.

4.3. Sea Surface Salinity climatology

Bulk ice salinity (S_{ice}) can be estimated from the underlying sea surface salinity (SSS) with an empirical function (Ryvlin et al., 1974) (see Eq. 1). There are global sea surface salinity products derived from SMOS satellite data. Ocean salinity is one of the two applications SMOS was originally designed for. However, SMOS-derived ocean salinity is not available in ice-covered regions. Therefore, we use SSS climatology based on the model outputs.

The Arctic SSS data used in this work result from an integration of the MIT general circulation model (MITgcm) including inter-annually varying surface forcing. From the model's daily surface salinity output for the years 2002-2009, a 'weekly climatology' was produced. It means that for every week in that climatological year, 56 salinity values (7 days x 8 years) were averaged at each location. The resulting climatology has therefore 52 values (52 weeks) at each position. In conclusion, we use a seasonal climatology with weekly resolution, which we have abbreviated to

'weekly climatology'. Figure 6 upper panel shows the mean and standard deviation of weekly SSS for winter seasons, based on the 8 yrs. of daily model output. SSS in the Laptev Sea, parts of the Kara Sea, and the Baltic Sea is much lower than that in the central Arctic due to the influence of river run-offs. In contrast, in Baffin Bay, the Greenland Sea, and the Barents Sea, SSS is higher than in the central Arctic. The mean weekly SSS in the Baltic sea varies in the range of 4–10 g/kg, in accordance to the observed climatology given in Janssen et al. (1999). To calculate Arctic-wide ice thickness distributions, it is necessary to use the spatially and temporally variable weekly SSS climatology.

SSS climatology in the Antarctic (Figure 6 lower panel) is based on the monthly model outputs of GECCO, a quasi-global simulation using MITgcm model over the years of 1952-2001. The model has a horizontal resolution of 1°x1°, with 23 vertical levels. In-situ measurements and satellite data are assimilated (Köhl and Stammer, 2008). In contrast to variable SSS distribution in the Arctic due to river run-offs, SSS in the Antarctic is almost constant, slightly varying between 33-35 g/kg, with a standard deviation less than 1 g/kg.
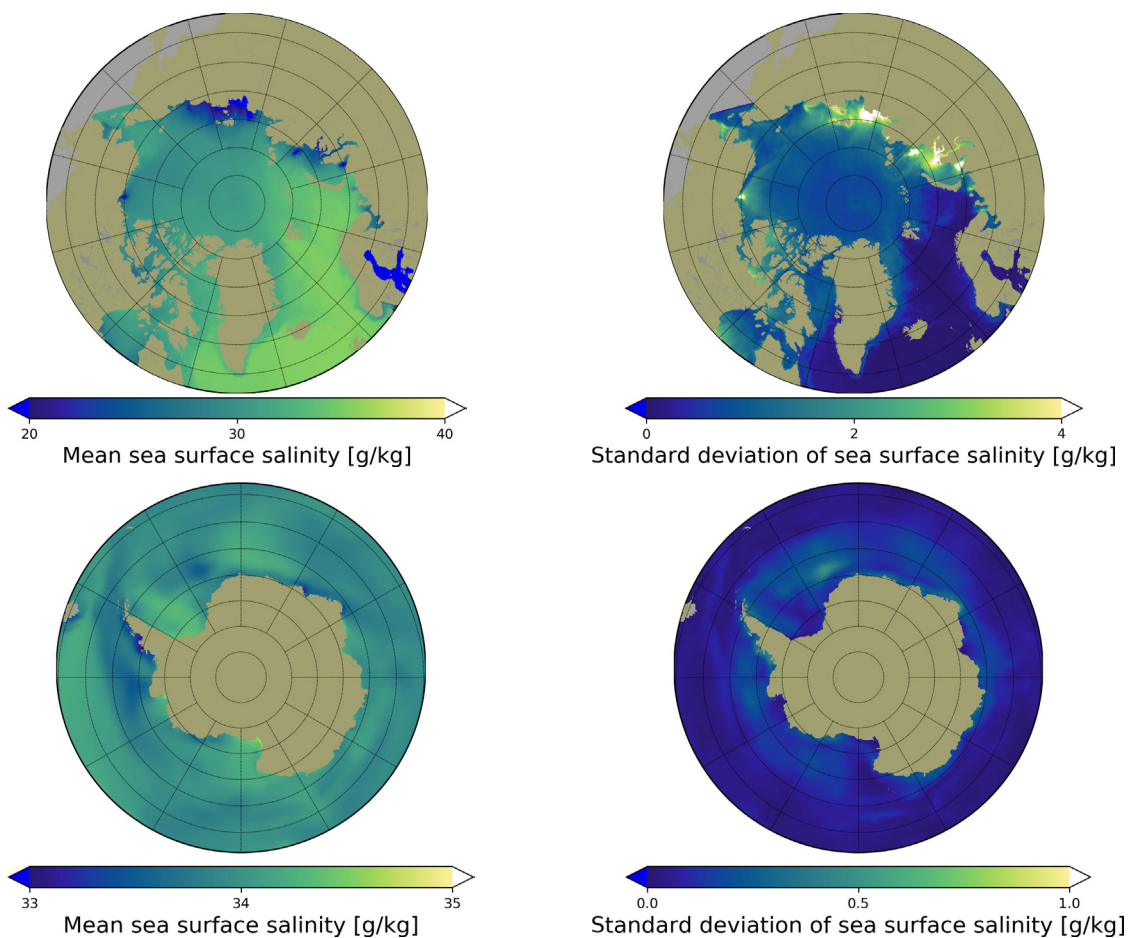

Figure 6. Mean (left column) and standard deviation (right column) of sea surface salinity in the Arctic (upper row) and in the Antarctic (bottom row). In the Arctic, the mean and standard deviation are calculated from 52 weeks sea surface salinity climatology and in the Antarctic they are from monthly climatology. Note that the colorbars have different scales.

4.4. Radiation model

The basis of the SMOS ice thickness retrieval is the sea ice radiation model adapted from Menashi et al., 1993. The sea ice radiation model consists of a plane ice layer bordered by the underlying sea water and air on the top. The model does not include snow layer. A snow layer has a twofold effect on the L-band emission. One is the thermodynamic insulation effect, which will be discussed in the following section, the other is the radiative contribution to the overall brightness temperature, which is not included in the current retrieval.

The brightness temperature over sea ice depends on the dielectric property of the ice layer which is a function of brine volume (Vant et al., 1978). The brine volume is a function of ice salinity and ice temperature (Cox et al., 1983). More details about the dielectric property and brine volume of the ice layer can be found in Kaleschke et al., 2010.

The first generation of SMOS sea ice thickness retrieval algorithms (Algorithm I) is a semi-empirical method which is based on two tie-points, one for open water one for thick ice, and a constant attenuation factor for a gamma function (Kaleschke et al., 2010, 2012). The two constant tie points were estimated from the observed SMOS brightness temperatures over open water and thick first year ice during the freezing period of 2010 in the Arctic. The constant attenuation factor was derived from the sea ice radiation model (Menashi et al., 1993) for a representative bulk ice temperature of -7°C and bulk ice salinity of 8 g/kg in the Arctic.

The observed brightness temperature depends on the fractional ice coverage, the temperatures of the sea and the ice, and their emissivities respectively. In addition, the signal is slightly attenuated by the atmosphere and includes the reflected sky background and RFI. In the following we neglect these additional contributions and assume a spatially homogeneous ocean that is either ice free or 100% covered by sea ice. By assuming a homogeneous dielectric-slab of thickness d_{ice} the emissivity is calculated according to Kaleschke et al., 2010. A semi-empiric approximation of the relationship between TB and d_{ice} is given by the following expression

$$TB = T_1 - (T_1 - T_0)\exp(-\gamma d_{ice}) \tag{1}$$

with the brightness temperatures of open water T_0 and infinitely thick sea ice T_1, and an attenuation factor $\gamma(T_{ice}, S_{ice})$. We call the parameters T_0 and T_1 tie points analogous to the denomination used for ice concentration algorithms. With the tie points and the attenuation factor we can calculate ice thickness from the observed brightness temperature. In Algorithm I we assumed the parameter γ as constant in time and space (Kaleschke et al., 2010). The plane layer ice thickness d_{ice} estimated with this method is used as initial ice thickness for the iterative ice thickness retrieval Algorithm v3.2 and v3.3.

Altorithm I has the advantage of easily to use without any auxiliary data. However, the sea ice emissivity varies with ice temperature and salinity. For a thin ice layer, the ice temperature gradient within the ice can be assumed to be linear (Maass 2013). Assuming that the water under sea ice is at the freezing point, we can calculate bulk ice temperature (T_{ice}) averaging the snow-ice interface temperature (T_{si}) and the freezing sea water temperature (T_w). Ice temperature and ice salinity measurements are rare and they are not continuously available on a daily basis. An alternative solution is therefore to derive these two parameters from auxiliary data during the sea ice thickness retrieval. The ice surface temperature is calculated with a thermodynamic model with surface air temperature (T_a) as boundary condition. The thermodynamic model is presented in the following section. Bulk ice salinity (S_{ice}) is estimated using the empirical function of Ryvlin (1974) (see Eq. 2).

$$S_{ice} = S_w(1 - S_R)e^{-a\sqrt{d_{ice}}} + S_R S_w \,, \tag{2}$$

where S_w is the SSS (derived from the SSS climatology as presented in section 4.3), d_{ice} is the plane layer ice thickness (here in cm) which is generated at each iteration step (Figure 9) in the retrieval model. S_R is the salinity ratio of the bulk ice salinity at the end of the ice growth season, , a is the

growth rate coefficient, which varies from 0.35 to 0.5. Ryvlin (1974) suggests using 0.5 for a and 0.13 for S_R. However, Kovacs (1996) compares the Ryvlin empirical equation with observed data in the Arctic and suggests using 0.175 for S_R instead of 0.13. In our model, we use 0.175 for S_R, which seems to fit better to the observation data of ice salinity in the Arctic. Cox and Weeks (1983) give another empirical relationship between S_{ice} and d_{ice} in the Central Arctic. The two empirical relationships have similar values for first year ice and a water salinity of S_w=31 g/kg (Kovacs, 1996). The S_{ice} in Eq. (1) is a function of the underlying SSS. Therefore, we can calculate ice salinity based on the SSS climatology.

The ice thickness retrieval with SMOS data is limited by the saturation of brightness temperature. We consider brightness temperature to reach saturation if the change of TB with ice thickness is less than 0.1 K per cm. Thus, TB of an ice layer with an ice temperature of -2°C and a salinity of 8 g/kg reaches its saturation for ice thicknesses of less than 30 cm, for example. This means that the maximal retrievable ice thickness (d_{max}) under warm and saline conditions can be as low as a few centimeters. On the contrary, under cold conditions and a low ice salinity, which is typical for coastal regions with river run-off, L-band brightness temperature emanates from a thicker ice layer. It reaches its saturation more slowly and maximal retrievable ice thickness is much higher (Figure 7). Therefore, SMOS ice thickness retrieval is more suitable for cold conditions and low ice salinity.
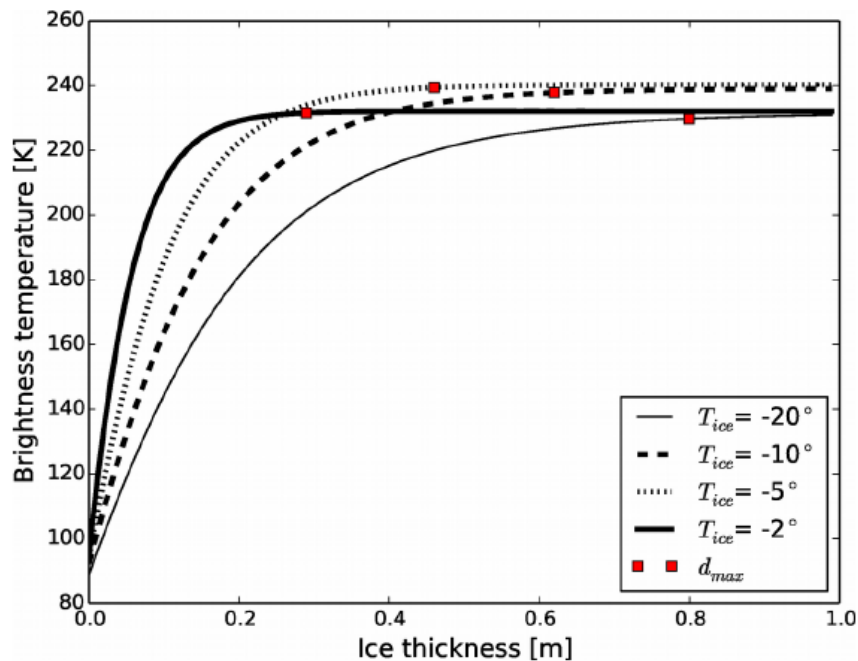
Figure 7. L-band Brightness temperature and sea ice thickness relationship under different ice temperature, simulated with the radiation model. Red dots show the maximal retrievable ice thickness under different ice temperature.

4.5. Thermodynamic model

Ice surface temperature is estimated from the ice thickness and surface air temperature using a thermodynamic model based on Maykut 1986. Thermal equilibrium is assumed at the surface of the ice layer. We apply our retrieval only for the winter period (for the northern hemisphere it is from October to April, for the southern hemisphere from April to October), which means that we can neglect the melting effects on the surface. Since we calculate daily averaged sea ice thickness of thin ice, it is a reasonable assumption to consider that the ice surface temperature is at equilibrium with the surface heat balance. Therefore, we use a heat flux balance equation and use the surface 2 metres air temperature from atmospheric reanalysis data as a boundary condition.

Although we neglect snow layer in the sea ice radiation model, we consider its thermal insulation effect in the thermodynamic model when we calculate the ice temperature. It is shown in Maass (2013) that the impact of a snow layer on the brightness temperature is partly caused by its insulation effect on the ice temperature. Snow is almost transparent in L-band and the radiative contribution is relatively small (Maass 2013). The insulation effect of a snow layer increases with snow thickness. Linear temperature gradient profiles are assumed for the ice and snow layers in the model. The snow thickness is calculated with ice thickness according to the relationship given in Doronin (1971).

$h_s = 0$ for $d_{ice} < 0.05$m,

$h_s = 0.05 \times d_{ice}$ for 0.05m$\le d_{ice} < 0.2$m,

$h_s = 0.09 \times d_{ice}$ for $d_{ice} \ge 0.2$m.

where d_{ice} is the sea ice thickness, h_s is the snow thickness. Under the assumption of thermal equilibrium, the incoming and outgoing heat fluxes compensate each other. The heat balance at the surface of a slab ice layer with thickness d_{ice} and a layer of snow with thickness h_s on top can be described as

$$(1 - \alpha)F_r - I_0 + F_{Lin} - F_{Lout} + F_s + F_e + F_c = 0 \tag{3}$$

where F_r is the incoming shortwave radiation, α is the albedo of the snow/ice layer, I_0 is the part of the incoming shortwave radiation that is transmitted into the ice, F_{Lin} is the incoming longwave radiation, F_{Lout} is the outgoing longwave radiation, F_s is the sensible heat flux, F_e is the latent heat flux, and F_c is the conductive heat flux. The radiative and turbulent fluxes $(1-\alpha)F_r - I_0$, F_{Lin}, F_{Lout}, F_e, and F_s are calculated as in Maykut (1986). $(1-\alpha)F_r - I_0$ is calculated based on the monthly net available shortwave radiation estimates (see Table 5.6 in Maykut, 1986). F_{Lin} and F_{Lout} are calculated with equation (4) and (6).

$$F_{Lin} = \varepsilon^* \sigma T_a^{\ 4} \tag{4}$$

$$\mathcal{E}* = 0.7855*\left(1 + 0.2232*C^{2.75}\right) \tag{5}$$

where ε^* is the effective longwave emissivity of atmosphere in the Arctic, C is cloud coverage, σ is the Stefan-Boltzman constant, and T_a is 2m surface air temperature.

$$F_{Lout} = \varepsilon_L \sigma T_s^{\ 4} \tag{6}$$

where ε_L is longwave emissivity of ice which is near 1, and T_s is the snow surface temperature.

Latent and sensible heat fluxes F_e and F_s are calculated with equation (7) and (8).

$$F_e = 0.622 \rho_a L C_e u (re_{sa} - e_{s0})/P \tag{7}$$

$$F_s = \rho_a c_p C_s u(T_a - T_s) \tag{8}$$

where ρ_a is the air density, r is the relative humidity, c_p is the specific heat of the air, C_s and C_e are the bulk transfer coefficient for sensible heat and latent heat, L is the latent heat of vaporization, P is the surface pressure. The saturation vapor pressure e_{sa} for air and e_{so} for ice are calculated with

$$e_s = 6.11*10^{\left(\frac{9.5t}{265.5+t}\right)} \tag{9}$$

where t is T_a and T_s in degree celsius.

The conductive heat flux F_c is given by equation (10), where k_s and k_i are the thermal conductivities of snow and ice, T_w is the freezing point of sea water, and T_s is the snow surface temperature. In the case of bare ice, T_s is the ice surface temperature. k_s is set to 0.31 W/m/K according to Yu and Rothrock (1996). The thermal conductivity of ice k_i is calculated with equation (11), bulk ice temperature T_{ice} with equation (12), and snow-ice interface temperature T_{si} with equation (13). To calculate T_{si} we need to know k_i. However, k_i is in turn a function of T_{ice}. As an approximation, we first calculate k_i with $0.5(T_s+T_w)$ instead of $0.5(T_{si}+T_w)$. Here we ignore the difference between T_s and T_{si}. This makes a minimal change in k_i. T_s is estimated with least-square method for each d_{ice} which is calculated from radiation model at each iteration step under the thermal equilibrium assumption (Figure 9). The units and detailed information about the variables and constants can be found in Table 1 and Table 2.

$$F_c = \frac{k_i k_s}{k_i h_s + k_s d_{ice}}(T_w - T_s) \tag{10}$$

$$k_i = 2.034 + 0.13\frac{S_{ice}}{T_{ice} - 273} \tag{11}$$

$$T_{ice} = 0.5(T_{si} + T_w) \tag{12}$$

$$T_{si} = \frac{T_s + \frac{k_i h_s}{k_s d_{ice}}T_w}{1 + \frac{k_i h_s}{k_s d_{ice}}} \tag{13}$$

4.6. Sea ice thickness distribution function

In the radiation model of (Menashi et al, 1993), a plane ice layer is assumed. However, natural sea ice exhibits a statistical thickness distribution within the spatial resolution of SMOS as a matter of the dynamic-thermodynamic growth and deformation processes. The brightness temperature measured by SMOS is a mixture of brightness temperatures from different ice thicknesses, and possibly open water. As SMOS brightness temperature is more sensitive to ice thicknesses less than 0.5 m, SMOS-derived sea ice thickness depends on the thin sea ice part in the sea ice thickness distribution within the spatial resolution while the contribution of the thicker sea ice part cannot be quantified due to the limited penetration depth. Thus, the overall mean thickness for a mixture of thin and thick sea ice can only be estimated in a statistical sense when the thickness distribution function is known. A possible solution for the corresponding underestimation of ice thickness is to correct the retrieved ice thickness using an ice thickness distribution function.

Sea ice deformation patterns are often described using self-similar functions such as the lognormal distribution. A theory of sea ice thickness distribution was developed by Thorndike et al., 1975. We use airborne sea ice thickness measurements in order to parameterize the thickness distribution function and to investigate the effect of the subpixel-scale heterogeneity on the thickness retrieval.

NASA's Operation IceBridge (OIB) airborne campaigns obtained large scale profiles of sea ice thickness derived from a laser altimeter system (Kurtz et al., 2013). We assume that the sea ice

thickness follows a lognormal distribution described in Eq. 14 (see detailed information in Tian-Kunze et al., 2014).

$$p(d_{ice}, \mu, \sigma) = \frac{1}{d_{ice}\sigma\sqrt{2\pi}} e^{-\frac{(\log(d_{ice})-\mu)^2}{(2\sigma^2)}}, \tag{14}$$

with the two parameters logmean (μ) and logsigma (σ). Furthermore, we assume a constant logsigma value (0.6 in Algorithm v3.2 and v3.3) to approximate the thickness distribution function with only one independent variable logmean. Under the assumption of a lognormal ice thickness distribution, the logmean is estimated comparing the calculated brightness temperature and the observed brightness temperature at each grid point (Eq. 15). The effect of the ice thickness distribution on brightness temperature is taken into account by the integration over the thickness range according to the superposition principle:

$$TB^*(d_{ice}) = \int_0^{\max(d_{ice})} TB(d_{ice})g(d_{ice})dd_{ice}, \tag{15}$$

with the thickness distribution function g(dice) and the brightness temperature of a single/plane-layer model TB(d_{ice}). g(dice) is the same as p(dice, μ, σ) under fixed logmean (μ) and logsigma (σ). Here d_{max} and max(d_{ice}) are two different parameters. While d_{max} is the maximum retrievable single layer ice thickness (see section 4.4), max(d_{ice}) is the maximum of ice thickness in the ice thickness distribution function. The brightness temperature weighted with the thickness distribution TB* suggests a sensitivity to ice thicknesses larger than d_{max}. Here d_{max} and d_{ice} both refer to the single-layer thickness. The real mean thickness denoted as H is calculated based on the ice thickness distribution function g(d_{ice}). H is strongly underestimated if the retrieval does not account for the thickness distribution. The overall effect can be explained as an apparently deeper penetration depth caused by the leading edge of the thickness distribution.

The implementation of a radiative transfer model that includes this effect is straightforward but computationally expensive because of the integration. A post-processing look-up table for the single-layer model has been generated to estimate an approximate correction factor. This method converts the single-layer thickness d_{ice} to the mean thickness H. The look-up table for the conversion from d_{ice} to H is generated using forward method. For each T_{ice} (ranging from 253.15K to 273.15K) and S_{ice} (ranging from 0 to 20 psu) we calculate TB for each d_{ice} ranging from 0 to 4m. We assume that the max(d_{ice}) is 4m for thin first year ice. As can be seen from Figure 8, for thin first year ice the ice thickness distribution function decreases sharply with ice thickness. Using the calculated TB and the constant parameter logsigma, we first estimate logmean and accordingly the ice thickness distribution function. The mean ice thickness H is calculated then with the ice thickness distribution function as weighting function on ice thickness range of 0-4m. From the radiation model and thermodynamic model described in section 4.4 and 4.5 we get the plane layer ice thickness d_{ice}, T_{ice} and S_{ice} at each grid point. With T_{ice}, S_{ice}, and d_{ice}, as input data we can read out the mean ice thickness H easily from the look-up table.

The implementation of a lognormal function is an approximation of the ice thickness distribution within the SMOS spatial resolution. This is an attempt to correct the underestimation of ice thickness caused by the plane ice layer assumption. However, there are uncertainties concerning the ice thickness distribution function and the determination of logsigma, which was derived from IceBridge data mainly over multi-year ice regions.
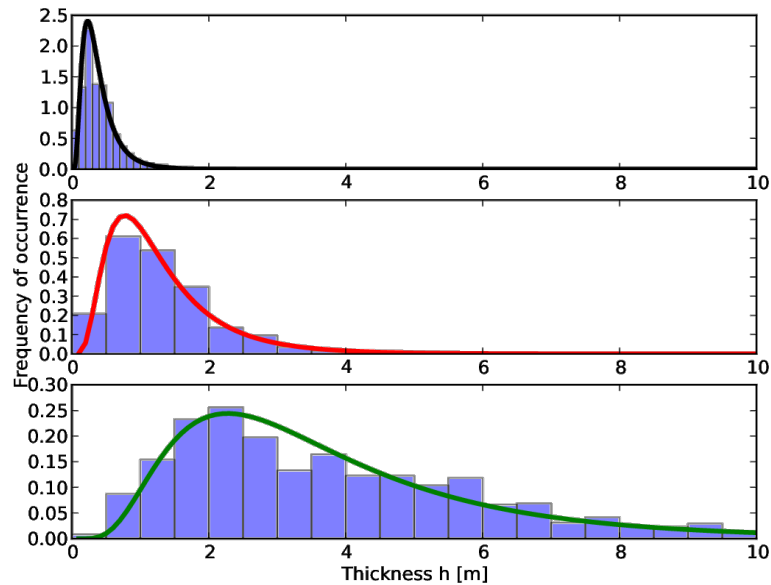
Figure 8. Sea ice thickness distribution derived from NASA's Operation IceBridge data from 2012 (lower panel) and 2013 (middle panel) and Laptev Sea 2014 (upper panel). The data is used to estimate the logsigma (σ) in the retrieval. More details about the sea ice thickness distribution can be found in Kaleschke (2017).

4.7. Iteration method

The advantage of the empirical method (Algorithm I, see section 4.4) is the retrieval of ice thickness from brightness temperatures without any auxiliary data set. However, the brightness temperature measured by a L-band radiometer over sea ice depends on the dielectric properties of sea ice which are functions of ice temperature and ice salinity, which means the assumption of constant retrieval parameters could cause considerable errors in the regions where these parameters strongly differ from the assumed constant values.

The challenge of using variable ice temperature and ice salinity is that both of them are in turn functions of ice thickness. The algorithm is based on the forward model consisting of the radiation and thermodynamic model. Therefore, we approximate ice thickness by repeating the radiation and the thermodynamic model until a convergence point is found for the solution (Figure 9). In this process, at each step ice temperature and ice salinity are calculated for the respective ice thickness approximation (see equation 12 and equation 2). The starting point of the iteration is the ice thickness estimated with semi-empirical method (Algorithm I). At each iteration step, we use ice thickness, ice temperature, and ice salinity to calculate brightness temperature with the radiation model. The calculated brightness temperature is then compared with that observed by SMOS. To minimize the difference between the observed and the calculated brightness temperatures, the new ice thickness is estimated with a linear approximation method. We define two stopping criteria for the iteration: a brightness temperature difference of less than 0.1 K, or an ice thickness difference of less than 1 cm. The first criterion is defined by considering the radiometric accuracy of the brightness temperature measurements and the number of daily available measurements. We apply the first criterion if the ice is thicker than 30 cm and otherwise the second criterion.

The maximal retrievable ice thickness is determined with the same criteria for the saturation of brightness temperature, i.e. that the brightness temperature change is less than 0.1 K per 1 cm ice thickness. We define a saturation factor as the ratio between ice thickness and maximal retrievable ice thickness. If the saturation factor reaches 100 %, it indicates that the estimated ice thickness is the minimum ice thickness of the pixel.

To optimize the computing time, lookup tables are generated by forward running the radiation and thermodynamic models in the range of possible surface air temperatures, SSS, wind velocities, and

net incoming shortwave radiations. This speeds up significantly the daily processing of sea ice thickness. Four different look-up tables are generated to speed up the retrieval.

1. Look-up table for the radiation model: For this look-up table we divided plane layer ice thickness d_{ice} into 300 bins ranging from 0-3m, T_{ice} from 253.15K to 273.15 in 200 bins, S_{ice} from 0 to 20psu in 200 bins. For each d_{ice}, T_{ice}, S_{ice} we run the radiation model (section 4.4) to get respective TB. This table is the basis to calculate maximal retrievable ice thickness d_{max}.

2. Look-up table for d_{max}: The sensitivity of brightness temperature to the ice thickness decreases with ice thickness. Kaleschke et al., 2012 has shown that the maximal retrievable ice thickness for plane ice layer is about 0.5m. This varies with T_{ice} and S_{ice}. We use the same T_{ice}, S_{ice} ranges as for the radiation model look-up table to calculate the upper limit of retrievable ice thickness with the criterion that the brightness temperature change is less than 0.1 K per 1 cm ice thickness change. Sea ice product provides at each grid the saturation ratio which is the ratio of d_{ice} and d_{max}. Ice thickness data with high saturation ratio has large uncertainties as well.

3. Look-up table for d_{ice} for given T_a, sea surface salinity (SSS), and TB: If we know T_{ice} and S_{ice}, we can easily read out d_{ice} from the first look-up table using observed TB. However, this is not the case. We need to calculate T_{ice} from T_a, S_{ice} from SSS. Since both T_{ice}, S_{ice} are functions of d_{ice}, we need the iteration method described in Figure 9. To speed up the retrieval, we run the iteration steps for all T_a and SSS which we can expect during winter seasons and save the results in the T_a-SSS-d_{ice} -TB look-up table.

4. Look-up table for the conversion from d_{ice} to H: This is described in section 4.6.
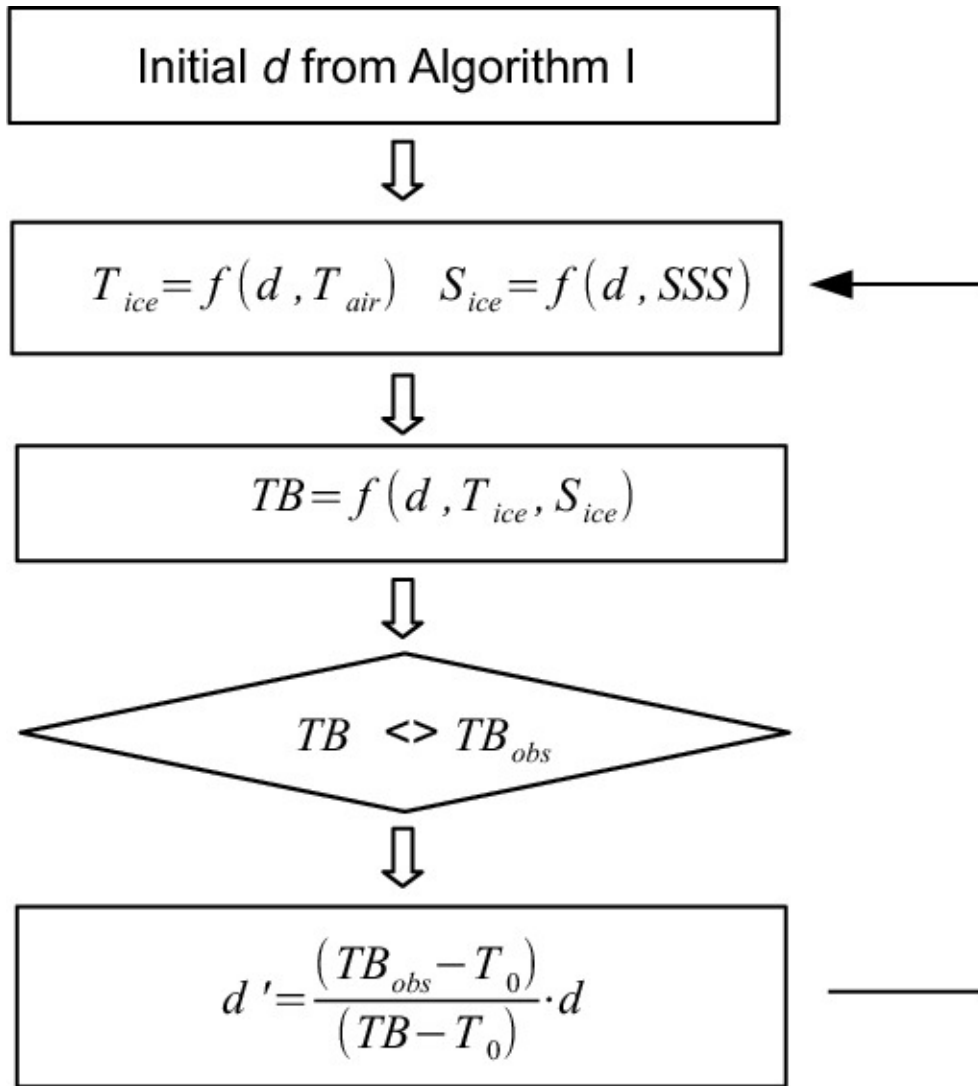
Figure 9. Schematic flow chart of the retrieval steps. d and d´ are the sea ice thicknesses d_{ice} from the consecutive steps, TB and TB_{obs} are calculated and observed brightness temperatures, and T_0 is the brightness temperature of sea water assumed to be 100.5 K.

4.8. Retrieval bias and uncertainties

We assume 100 % ice coverage for simplicity. This causes systematic underestimation of sea ice thickness where the assumption does not meet. The brightness temperature over ice-sea water mixed areas can be described as

$$TB = TB_{water} \times (1 - IC) + TB_{ice} \times IC, \qquad (16)$$

where IC is the ice concentration, TB_{water} and TB_{ice} are the brightness temperatures over sea water and ice, respectively.

SMOS brightness temperature over sea water shows a stable value of about 100.5 K with a standard deviation of about 1 K in the Arctic region. With this constant brightness temperature over open water, we can calculate brightness temperature over ice using ice concentration charts from passive

microwave radiometer data. During the winter most of the ice-covered area in the Arctic has ice concentration higher than 90 % (Andersen et al., 2007). The passive microwave radiometer ice concentration charts have an uncertainty of 5 % in the winter time. At high concentrations, correcting the retrieved ice thickness with ice concentration data set with an uncertainty of 5 % can cause higher errors than the 100 % ice coverage assumption (Tian-Kunze et al., 2014). Therefore, we assume in the retrievals a 100 % ice coverage. This systematic bias caused by this assumption increases exponentially with decreasing ice concentration.

There are several factors that cause uncertainties in the sea ice thickness retrieval: the uncertainty of the SMOS brightness temperature, the uncertainties of the auxiliary data sets, and the assumptions made for the radiation and thermodynamic models.

For our purpose we average TB over the incidence angle range of 0°-40°. There are mostly more than 100 TB measurements at each grid point in the Arctic region per day. By averaging the measurements, we reduce on the one hand the measurement uncertainty, on the other hand smooth out the temporal and spatial variation. We describe the variability of TB by dividing the standard deviation of TB with the square root of the number of measurements during one day at each grid point. This is mostly less than 0.5 K in the Arctic, except for the strongly RFI affected regions.

The uncertainties of T_{ice} and S_{ice} depend on the uncertainties in the T_a and SSS and the uncertainty caused by the missing physics. Both T_a and SSS are derived from model outputs. Due to the sparse observations in the polar regions, T_a and SSS themselves contain large uncertainties. As a first approximation we assume 1 K for the standard deviation of T_{ice} which is estimated with standard deviation of T_a during winter season. More investigations should be conducted to better estimate the uncertainty in T_{ice} in the future. The different error factors are not independent, because they are functions of ice thickness. At present, each error caused by the standard deviations of brightness temperature, ice salinity, and ice temperature is estimated by keeping the other parameters constant. The total uncertainty given in the data set is the sum of these errors. Errors caused by the assumptions about fluxes and snow thickness have not yet been included. The impact of snow cover on the ice thickness retrieval can be better understood by carrying out elaborate in-situ measurements as done during MOSAiC campaign. This remains as future work.

Considering the difficulty to estimate the uncertainties in the radiation and thermodynamic models, as well as in the parameters calculated from the auxiliary data, we combined the sea ice thickness uncertainty with the sea ice thickness based on the very first analysis of uncertainties with standard deviations of T_{ice}, S_{ice}, and TB. Figure 10 shows the sea ice thickness uncertainty provided in the data of 1st December, 2020. Ice thickness uncertainty increases rapidly with sea ice thickness. The uncertainties provided in the current data set are the very first estimations. An elaborate investigation about the correlation between these error factors is an on-going work.
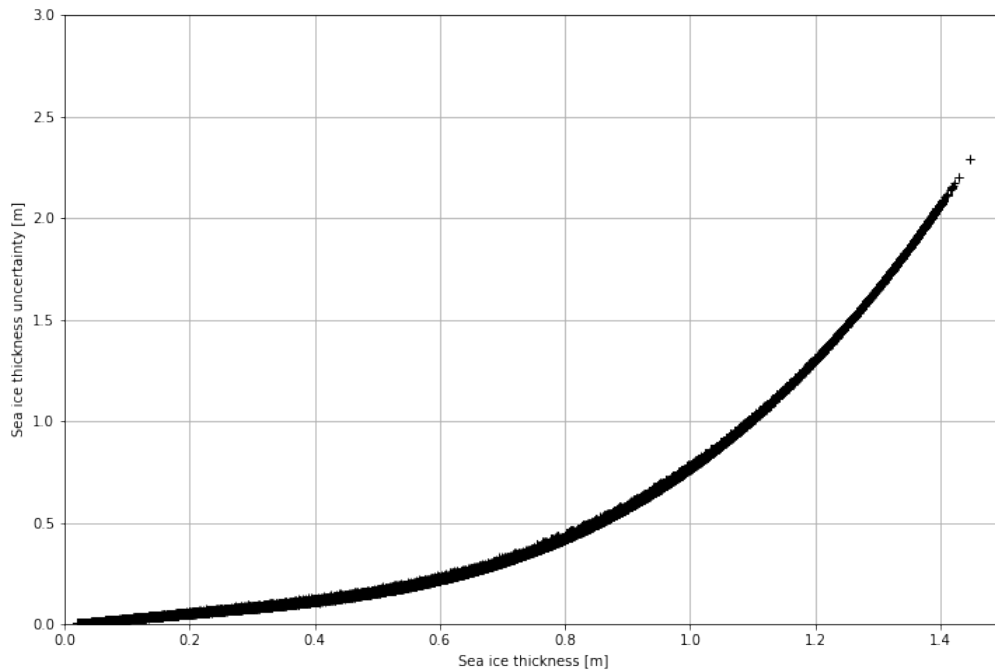
Figure 10. Sea ice thickness uncertainty provided in the sea ice product v3.3. Date: 1st December, 2020.

4.9. Antarctic sea ice thickness product

Sea ice thickness in the Antarctic is still a preliminary product. Although it is derived with the same retrieval algorithm as in the Arctic, the situation in the Antarctic is more complicated and more uncertain. First, ice drift is much faster in the Antarctic due to missing land boundaries. This leads to enhanced convergence and divergence activities within the ice, hence more openings. As mentioned earlier, we assume 100% ice coverage in the retrieval. In the Arctic, except for the marginal ice zone, ice concentration is almost 100%. However, in the Antarctic the low ice concentration can lead to significant underestimation of ice thickness. Second, due to heavy snow fall, ice layer in the Antarctic suffers often under flooding, which leads to flooded snow-ice layer which can significantly alter the dielectric property of snow layer. To simulate the brightness temperature over such flooded snow-ice layer remains as a difficult, unsolved problem due to lacking knowledge of snow layer in the Antarctic. Furthermore, the monthly sea surface salinity climatology in the Antarctic is based on GECCO2 ocean reanalysis (see section 4.3) with much coarser horizontal resolution.

5. Product description

Daily sea ice thickness data have been generated at AWI with one day latency for winter seasons: from mid-October to mid-April in the Arctic. Table 5 shows the overview of operational SMOS product, which is disseminated via:

Public: ftp://ftp.awi.de/sea_ice/product/smos/

ESA: https://smos-diss.eo.esa.int/

Detailed product description can be found in

https://spaces.awi.de/display/CS2SMOS/SMOS+Sea+Ice+Thickness.

Table 5. Overview of operational SMOS product

Parameter	Sea ice thickness
Spatial coverage	Northern hemisphere, poleward of 50°N, -180°E to 180°E
Spatial resolution	12.5 km x 12.5 km
Temporal coverage	Northern hemisphere, 15. Oct.-15. Apr. 2010 to present
Temporal resolution	1 day
Data format	NetCDF v4
Platforms	SMOS
Current version	V3.3

6. References

Andersen, S., Tonboe, R., Kaleschke, L., Heygster, G., and Peder- sen, L.: Intercomparison of passive microwave sea ice concen- tration retrievals over the high-concentration Arctic sea ice, J. Geophys. Res., 112, C08004, doi:10.1029/2006JC003543, 2007.

Bertino, L. and Lisæter, K. A.: The TOPAZ monitoring and predic- tion system for the Atlantic and Arctic Oceans, Journal of Oper- ational Oceanography, 1, 15–19, 2008.

Burke, W., Schmugge, T., and Paris, J.: Comparison of 2.8-and 21- cm microwave radiometer observations over soils with emission model calculations, J. Geophys. Res., 84, 287–294, 1979.

Camps, A., Vall-llossera, N., Duffo, N., Torres, F., and Corbella, I.: Performance of sea surface salinity and soil moisture retrieval al- gorithms with different auxiliary datasets in 2-D L-band aperture synthesis interferometric radiometers, IEEE T. Geosci. Remote, 43, 1189–1200, doi:10.1109/TGRS.2004.842096, 2005.

Cox, G. and Weeks, W.: Equations for determining the gas and brine volumes in sea-ice samples, J. Glaciol., 29, 306–316, 1983.

Doronin, Y.: Thermal interaction of the atmosphere and the hydro- sphere in the Arctic, CoronetBooks, Philadelphia, 1971.

Haas, C., Lobach, J., Hendricks, S., Rabenstein, L., and Pfaffling, A.: Helicopter-borne measurements of sea ice thickness, using a small and lightweight, digital EM system, J. Appl. Geophys., 67, 234–241, 2009.

Helm, V., Hendricks, S., Göbell, S., Rack, W., Haas, C., Nixdorf, U., & Boebel, T. (2006). Cryovex 2004 and 2005 (bob) data acquisition and final report. Bremerhaven, Germany: Alfred Wegener Institute.

Kaleschke, L., Maaß, N., Haas, C., Hendricks, S., Heygster, G., and Tonboe, R. T.: A sea-ice thickness retrieval model for 1.4 GHz radiometry and application to airborne measurements over low salinity sea-ice, The Cryosphere, 4, 583–592, doi:10.5194/tc-4- 583-2010, 2010.

Kaleschke, L., Tian-Kunze, X., Maaß, N., Mäkynen, M., and Dr- usch, M.: Sea ice thickness retrieval from SMOS brightness tem- peratures during the Arctic freeze-up period, Geophys. Res. Lett., 39, L05501, doi:10.1029/2012GL050916, 2012.

Kaleschke. L. (2013). SMOS Sea ice retrieval study (SMOSSIce): Final report. ESA ESTEC Contract No: 4000101476/10/NL/C. Zenodo. https://doi.org/10.5281/zenodo.3406130

Kaleschke. L. (2017). ESA Support To Science Element (STSE) SMOS+Sea Ice Final Report EUROPEAN SPACE AGENCY STUDY CONTRACT REPORT UNDER ESTEC CONTRACT No. 4000112022/14/I-AM. Zenodo. https://doi.org/10.5281/zenodo.3406134

Kaleschke et al., "SMOS sea ice product: Operational application and validation in the Barents Sea marginal ice zone", Remote Sensing of Environment, 180 (2016) 264-273, doi:10.1016/j.rse.2016.03.009

Kerr, Y., Waldteufel, P., Wigneron, J., Martinuzzi, J., Font, J., and Berger, M.: Soil moisture retrieval from space: The Soil Moisture and Ocean Salinity (SMOS) mission, IEEE T. Geosci. Remote, 39, 1729–1735, 2001.

Köhl A. and D. Stammer (2008), Variability of the Meridional Overturning in the North Atlantic from the 50 years GECCO State Estimation, J. Phys. Oceanogr., 38, 1913-1930.

Kurtz, N. T., Farrell, S. L., Studinger, M., Galin, N., Harbeck, J. P., Lindsay, R., Onana, V. D., Panzer, B., and Sonntag, J. G.: Sea ice thickness, freeboard, and snow depth products from Oper- ation IceBridge airborne data, The Cryosphere, 7, 1035–1056, doi:10.5194/tc-7-1035-2013, 2013.

Kwok, R. and Cunningham, G.: ICESat over Arctic sea ice: Esti- mation of snow depth and ice thickness, J. Geophys. Res., 113, C08010, doi:10.1029/2008JC004753, 2008.

Laxon, S., Peacock, N., and Smith, D.: High interannual variability of sea ice thickness in the Arctic region, Nature, 425, 947–950, 2003.

Laxon, S. W., Giles, K. A., Ridout, A. L., Wingham, D. J., Willatt, R., Cullen, R., Kwok, R., Schweiger, A., Zhang, J., Haas, C., Hendricks, S., Krishfield, R., Kurtz, N., Farrell, S., and Davidson, M.: CryoSat-2 estimates of Arctic sea ice thickness and volume, Geophys. Res. Lett., 40, 732–737, doi:10.1002/grl.50193, 2013.

Maass, N.: Remote sensing of sea ice thickness using SMOS data, Reports on Earth System Science, available at: http://www.mpimet.mpg.de/fileadmin/publikationen/Reports/ WEB_BzE_131.pdf (last access: 26 May 2014) 2013

Maekynen, M., Cheng, B., and Similae, M.: On the accuracy of thin-ice thickness retrieval using MODIS thermal im- agery over Arctic first-year ice, Ann. Glaciol., 62, 87–96, doi:10.3189/2013AoG62A166, 2013.

Maykut, G. A.: Geophysics of Sea Ice, chap. The surface heat and mass balance, 395–463, Plenum, New York, 1986.

Mecklenburg, S., Drusch, M., Kerr, Y. H., Font, J., Martin-Neira, M., Delwart, S., Buenadicha, G., Reul, N., Daganzo-Eusebio, E., Oliva, R., and Crapolicchio, R.: ESA's soil moisture and ocean salinity mission: mission performance and operations, IEEE T. Geosci. Remote, 50, 1354–1366, 2012.

Menashi, J., Germain, K., Swift, C., Comiso, J., and Lohanick, A.: Low-frequency passive-microwave observations of sea ice in the Weddell Sea, J. Geophys. Res., 98, 22569–22577, 1993.

Pfaffling, A., Haas, C., and Reid, J. E.: Direct helicopter EM-Sea- ice thickness inversion assessed with synthetic and field data, Geophysics, 72, F127–F137, 2007.

Ricker, R. , Hendricks, S. , Kaleschke, L. , Tian-Kunze, X. , King, J. and Haas, C. (2017): A weekly Arctic sea-ice thickness data record from merged CryoSat-2 and SMOS satellite data , Cryosphere,11 (4), pp. 1607-1623 . doi: 10.5194/tc-11-1607-2017

Ryvlin, A. I.: Method of forecasting flexural strength of an ice cover, Probl. Arct. Antarct., 45, 79–86, 1974.

Schmitt, A.U.; Kaleschke, L. A Consistent Combination of Brightness Temperatures from SMOS and SMAP over Polar Oceans for Sea Ice Applications. *Remote Sens.* **2018**, *10*, 553.

Sobjaerg, S., Kristensen, S., Balling, J., & Skou, N. (2013). The airborne EMIRAD L-band radiometer system. Geoscience and Remote Sensing Symposium (IGARSS), 2013 IEEE International (pp. 1900–1903). http://dx.doi.org/10.1109/IGARSS.2013.6723175.

Thorndike, A.: Estimates of sea ice thickness distribution using ob- servations and theory, J. Geophys. Res., 97, 12601–12612, 1992. Thorndike, A., Rothrock, D., Maykut, G., and Colony, R.: The thickness distribution of sea ice, J. Geophys. Res., 80, 4501– 4513, 1975.

Tian-Kunze, X., Kaleschke, L., Maaß, N., Mäkynen, M., Serra, N., Drusch, M., & Krumpen, T. (2014). SMOS-derived thin sea ice thickness: Algorithm baseline, product specifica- tions and initial verification. The Cryosphere, 8, 997–1018. http://dx.doi.org/10.5194/ tc-8-997-2014 (URL: http://www.the-cryosphere.net/8/997/2014/).

Vant, M., Ramseier, R., and Makios, V.: The complex-dielectric constant of sea ice at frequencies in the range 0.1–40 GHz, J. Appl. Phys., 49, 1264–1280, 1978.

Warren, S. G., Rigor, I. G., Untersteiner, N., Radionov, V. F., Bryaz- gin, N. N., Aleksandrov, Y. I., and Colony, R.: Snow depth on Arctic sea ice, J. Climate, 12, 1814–1829, 1999.

Yu, Y. and Rothrock, D.: Thin ice thickness from satellite thermal imagery, J. Geophys. Res., 101, 25753–25766, 1996.

Zhang, J. and Rothrock, D.: Modeling global sea ice with a thick- ness and enthalpy distribution model in generalized curvilinear coordinates, Mon. Weather Rev., 131, 845–861, 2003.

End of Document